Northumbria Research Link

Morphological Transitions of Water Channels Induced by Vertical Vibrations

Paolo Sartori[a], Luca Bonato[a], Giorgio Delfitto[a], Matteo Pierno[a], Giampaolo Mistura[a]*, Ciro Semprebon[b] and Martin Brinkmann[c†]

[a] Dipartimento di Fisica e Astronomia "G. Galilei", Università di Padova, Via Marzolo 8, I-35131 Padova, Italy
[b] Department of Physics, Durham University, Durham, DH1 3LE, UK
[c] Geometry of Interfaces group, Experimental Physics, Saarland University, 66123 Saarbrücken, Germany

ABSTRACT: We report the results of comprehensive experiments and numerical calculations of interfacial morphologies of water confined to the hydrophilic top face of rectangular posts that is subject to vertical vibrations. In response to the mechanical driving, an initially flat liquid channel is collected into a liquid bulge that forms in the center of the rectangular post if the acceleration exceeds a certain threshold. The bulge morphology persists after the driving is switched off in agreement with the morphological bi-stability of static interfacial shapes on posts with large length to width ratios. In a narrow frequency band, the channel does not decay into a bulge at any acceleration amplitude, and displays irregular capillary waves and sloshing instead. On short posts, however, a liquid bulge can be dynamically sustained through vertical vibrations but quickly decays into a homogeneous channel after the external driving is stopped. To explain the dynamic bulging of the liquid interface, we propose an effective lifting force pulling on the drop's slowly moving center of mass in the presence of fast oscillation modes.

INTRODUCTION

Resonant oscillations of sessile drops have been the subject of recent experimental and numerical studies because of their relevance to microfluidic applications, in particular to mixing and actuation. In contrast to electrowetting[1] and magnetic actuation[2] which require polar liquids or ferrofluids, respectively, mechanical vibrations couple to drop inertia and, thus, provide an universal driving mechanism for all types of liquids. Taking advantage of the rectifying effect related to a contact angle hysteresis, horizontal and vertical vibrations with a controlled phase shift can be utilized for directed drop actuation and let drops even climb against gravity.[3–10] Similarly, spatio-temporal modulation of the levitation acoustic field allows continuous planar transport and processing of droplets.[11]

Recent investigations have shown that topographic micro-pattern of linear grooves and ridges may increase the yield of passive fog collectors.[12] During growth, the droplets wetting the ridges coalesce and may form stretched out, linear morphologies, called filaments, or are collected into larger droplets which facilitates droplet shedding by gravity or other external forces. The transition between the flat channel or filament-like morphology and the localized, droplet-like bulge morphology is controlled by surface wettability[13] and the geometry of the ridges.[14]

More generally, static interfacial shapes of sessile liquid drops wetting chemical or topographic surface patterns have been widely studied both at the applied[15,16] and fundamental levels.[13,14,17–22] Small drops wetting a rectangular stripe or annular ring, in particular, can be morphologically bi-stable in a certain range of liquid volumes.[14,23,24] In the latter cases, the interface of a drop in mechanical equilibrium may be found either in a flat, spread-out "channel" morphology or in a localized
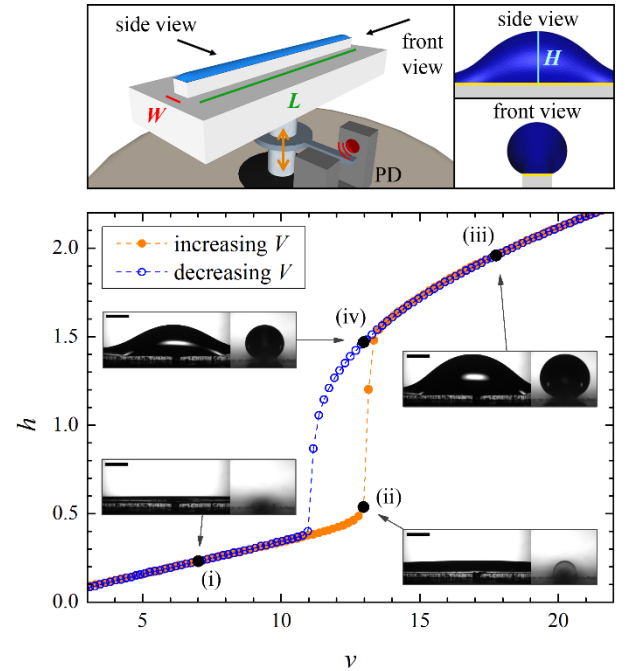
Figure 1 (Top) Sketch of the rectangular post attached to the shaft of the shaker (left); side and front views of the channel in the bulge state. The post is made out of PDMS. The top face in contact with water is covered with a gold layer. PD is the photo-dector to measure the vertical displacement. (Bottom) Reduced height $h = H/W$ of a water layer deposited on rectangular post of aspect ratio $\ell = 36$ as a function of the reduced volume $v = V/W^3$. Full (empty) symbols represent the experimental data during injection (extraction). The snapshots show the side and front images of the water channels taken at selected points along the height curve. The scale bars correspond to 0.5 mm.
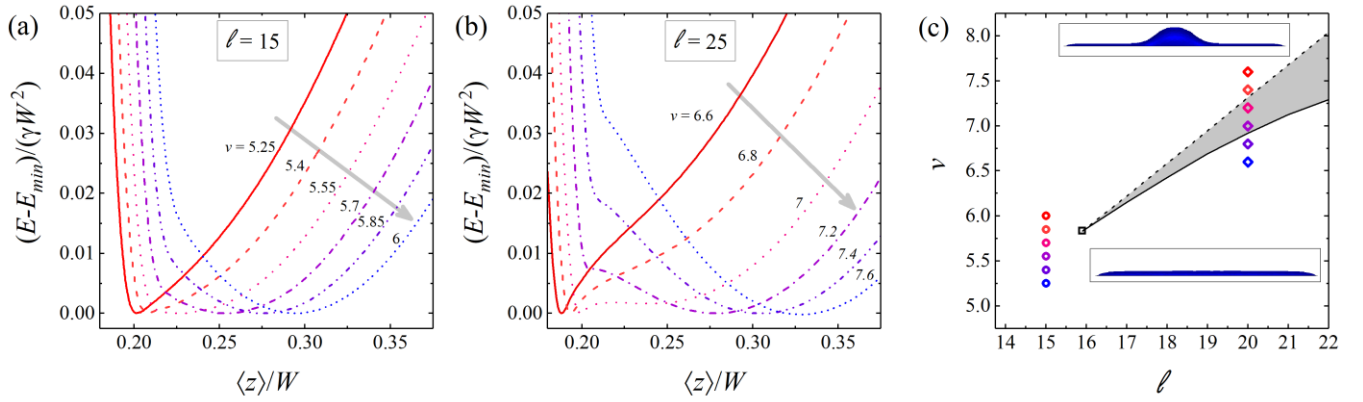
Figure 2 Energy landscapes of droplets in terms of the height $\langle z \rangle$ of the drop's center of mass above the post for a series of reduced liquid volumes v for short (a) posts $\ell = 15$ and long (b) posts $\ell = 25$. For the sake of comparison, each curve is shifted individually on the ordinate such that the minimum energy equals to zero. The gray arrows point into the direction of increasing volume. (c): Morphology diagram around the bifurcation point at $(\ell, v) \simeq (16, 5.8)$ (black square). Open circles (short posts) and diamonds (long posts) are the reduced volumes of the drops corresponding to the energy configuration shown in panels (a) and (b), respectively. The bi-stable region of control parameters is shown in gray. Channels become unstable on the dashed line while the bulges decay when crossing the solid line.

drop-like "bulge" morphology. Close to the point of instability, the energy barrier separating these two interfacial conformations is small, and one can expect that the transition from the meta-stable state into the global energy minimum can be easily triggered by external stimuli like mechanical vibrations of the underlying substrate.

The present work is the natural prosecution of our static study on rectangular posts[14] and demonstrates that vibrations can indeed induce a transition from a flat channel into the localized bulge, but this transition is inhibited under certain conditions. In a small range of vibration frequencies, the liquid interface of the channel does not decay into a liquid bulge but instead displays patterns of standing capillary waves with pronounced beating and highly irregular local amplitudes.

Interfacial shapes of the channel and bulge states obtained in numerical energy minimizations allowed us to compute the spectrum of natural frequencies for small amplitude oscillations using a boundary integral approach. The numerically computed oscillation modes of the bulge state not only agree with video recordings of the interfacial contours of forced oscillation modes in our experiments but also explain the generation of an effective dynamic force acting on the liquid during vertical vibrations. This upward directed force can be rationalized by the de-tuning of resonating oscillation modes during a redistribution of liquid in the drop wetting the post.

EXPERIMENTAL METHODS

Individual posts in polydimethilsiloxane (PDMS) having a rectangular cross-section, height $\sim$ 100 μm, width W = 500 μm, length L = 7 mm or 18 mm, and with a through hole of diameter $\approx$ 150 μm in the center, are fabricated following the same procedure used before.[14] The patterned sample is at-

tached to the moving shaft of an electromagnetic shaker as shown in Figure 1. The vibration amplitude A is determined with an IR photodetector (PD) that has been calibrated by optically measuring the net displacement of the shaft. The resolution in A is estimated to be 2 μm. The vertical acceleration is calculated from the formula $a = 4\pi^2 f^2 A$, where f is the vibrating frequency. With a feedback circuit, it is also possible to sweep f while maintaining A constant over a frequency interval $\sim$ 500 Hz. The PDMS posts are hydrophobic with a contact angle for water $\theta_0 = 110°$. Their top face is covered with a thin gold layer. To protect the vertical walls during the metallic deposition, they are covered with a UV curable optical adhesive, NOA 61.[25] Right before each measurement, the gold surface is activated in an ozone cleaner and then the cured NOA 61 coating is peeled off. As a result, the material contact angle on the top face is reduced to $\theta_0 \sim 15°$ and remains stable for a couple of hours. The central hole is connected to a thin tube attached to a syringe pump in series with a flow meter.

RESULTS AND DISCUSSION

Bistability of equilibrium shapes. Water drops of fixed volume V deposited on a perfectly wettable rectangular stripe of width W and length $L \gg W$ can assume two mechanically stable morphological states[13,14,17,23] with different height H (for the definition of the quantities c.f. also the top panel of Figure 1). If the vertical extension of the interface is small compared to the capillary length $L_c = \sqrt{\gamma/(g\rho)} \approx 2.7$ mm for water, gravity can be neglected and the stability of the shape is controlled only by the reduced volume of the drop, $v \equiv V/W^3$ and the aspect ratio $\ell \equiv L/W$, as outlined in Ref.[14] For small reduced volumes v, the liquid assumes the shape of a channel with a uniform cross section while, for large volumes, the liquid interface displays a central bulge.

2
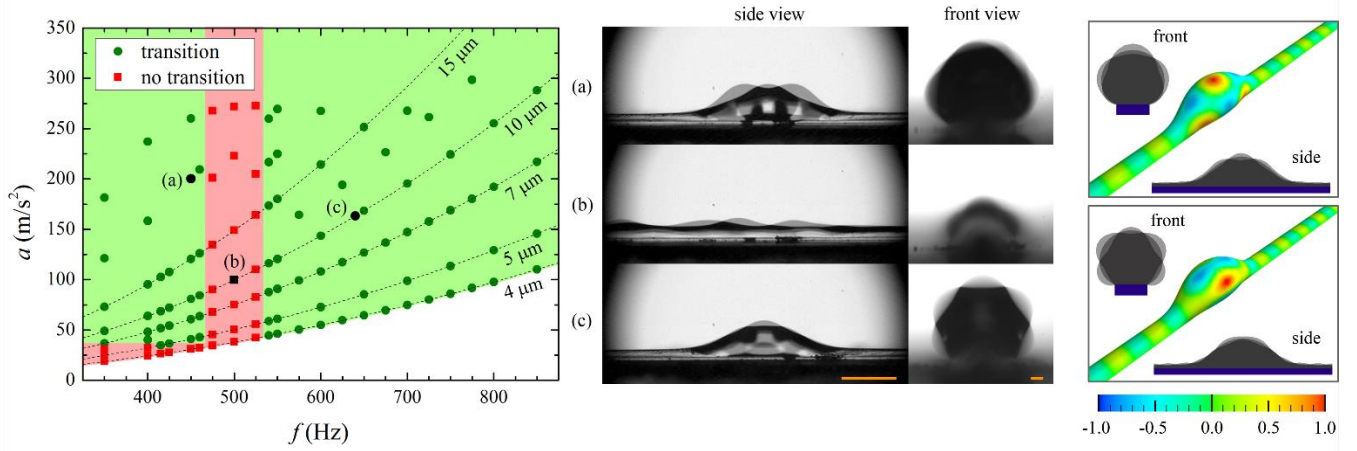
Figure 3 (Left) Dynamic phase diagram of the transition from the channel to the bulge state induced by vertical vibrations of frequency f and peak acceleration a. In the red region the system remains in the homogeneous channel state. Dashed lines indicate frequency sweeps of constant amplitude. The white region corresponds to oscillation amplitudes too small to be accurately measured. (Center) Side and front images of the channel profile taken at selected points in the phase diagram. For (a) and (c) the transition occurred and the system is in the bulge state. For (b) the system remains in the homogeneous channel state. The scale bars in the side view and in the front view correspond to 1 mm and 100 μm, respectively. (Right) Comparison with numerically computed oscillation modes resembling the modes shown in (a) and (b). The color map encodes local normal interfacial displacement rescaled by the maximum amplitude of the mode. Note that the sign is arbitrary.

The plot in Figure 1 shows the reduced height $h \equiv H/W$ as a function of the reduced water volume $v \equiv V/W^3$. Full (empty) symbols represent data during injection (extraction) of water. The plot in Figure 1 is complemented by images of the water profile taken at particular points as indicated in the graph. The observed shape transition is in agreement with a previous experimental study of water condensing on long posts.[14] Starting at small, reduced volumes, the water distributes evenly on the top face of the post, forming a liquid "channel" with a homogeneous, circular cross-section, c.f. Figure 1(i) and (ii). Noticeable deviations of this almost homogeneous profile occur only in the vicinity of the ends of the post and decay on a length scale comparable to the post width. Upon increasing the volume further, the radius of the circular segment decreases while the water interface forms a central bulge, which grows with v (Figure 1(iii)). The bulge formation is characterized by a pronounced increase in the reduced height h of the interface above the post, c.f. Figure 1(iv).

The transition from the channel to the bulge can be reversed upon decreasing the volume. It is apparent from Figure 1 that the volume v_{min} at the point where the bulge state spontaneously transforms back into a channel is smaller than the volume v_{max} where the channel transforms into the bulge. The bistable range of volumes and the corresponding hysteresis of the order parameter h is a clear indication that the observed morphological transition in Figure 1 is discontinuous.

However, on short posts with a length-to-width ratio smaller than $\ell^* \approx 16$, a continuous transition from the channel to the bulge morphology is observed.[14] The transition from a continuous to a discontinuous shape transformation, and the existence of a mechanically bistable region can be best understood by considering the qualitative changes of the energy landscape that the confined liquid drop experiences. To this end, we numerically computed local energy minima under the constraint of a fixed height of the center of mass $\langle z \rangle$ of the liquid drop above the top face of the post at $z = 0$. Our constrained energy minimizations show that the maximum height of the drop h is a monotonous function of $\langle z \rangle/W$ for every length to width ratio ℓ and, thus, is equivalently suited as an order parameter. Both quantities, h and $\langle z \rangle/W$, distinguish the bulge morphology from the liquid channel. To construct an energy landscape of the interfacial shapes on the post, the constrained energy minimizations were repeated for a series of reduced volumes v for a given value of ℓ.

The examples of the energy landscapes shown in Figure 2 illustrate the qualitative differences between a short post with $\ell = 15 \lesssim \ell^*$ and a long posts with $\ell = 25 > \ell^*$. Each local minimum on a curve in the plots Figure 2(a) and (b) correspond to mechanically stable interfacial shapes for the particular reduced volume v. Local maxima in between two local minima are saddle points in the energy landscape. The energy differences between the local minima and the saddle point represent the smallest work that needs to be injected to the liquid body to transform the shape into the other morphology. It is evident from Figure 2(a) that there is only one local minimum for any volume v if the length to width ratio is fixed to $\ell = 15$.

3
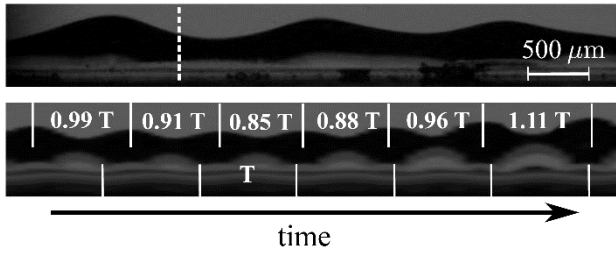
Figure 4 (Top) Snapshot of the irregular surface oscillations of a liquid channel state whose frequency $f \approx 500$ Hz lies in the gap of the dynamic phase diagram shown in Figure 3 (left). (Bottom) Time evolution of the channel profile along the cut indicated as a dashed line in the top snapshot. Bottom tics represent time intervals equal to the period T of the imposed vertical vibrations. Top tics highlight the intervals of the fast oscillations over slow "sloshing" modes in units of T.

However, on the long posts with $\ell = 25$ we observe a single local minimum only for small and large reduced volumes v. The plots in Figure 2(b) reveals a range of intermediate volumes where two local minima exist. The local energy minimum at the smaller value of $\langle z \rangle$ corresponds to a liquid channel while the one for larger $\langle z \rangle$ corresponds to a bulge morphology. If the reduced volume v exceeds a certain threshold value v_{max}, the local minimum of the channel disappears and the bulge morphology represents the only possible stable equilibrium state. Similarly, if the volume v falls below a threshold value $v_{min} < v_{max}$, the bulge state disappears leaving only channels as possible stable equilibrium states. The stability diagram shown in Figure 2(c) displays the region of mechanical bistability and the lines where channel and bulge morphologies become unstable during an increase or decrease of the volume v. Here, we focus on posts with length ℓ and volumes v around the bifurcation point at $(\ell^*, v^*) \simeq (16, 5.8)$ computed in Ref.[14].

The second derivative of the interfacial energy plotted in Figure 2(a) and (b) with respect to the coordinate $\langle z \rangle$ can be thought of as an effective spring constant of the liquid interface. This capillary spring becomes the softer, the closer the interfacial shape is to an instability. It is rather self-evident that the energy required to cross the energy barrier from the channel state to the bulge can be furnished by vertical vibrations of the supporting substrate, provided the channel state is sufficiently close to the point of instability v_{max}. Vertical vibrations applied to liquid channel on short posts, however, cannot permanently change the liquid shape because the liquid conformation will always return into the single energy minimum. Sufficiently close to the bifurcation point in the region of single minima for $\ell < \ell^*$, the capillary spring is soft while the drop cannot decay into another conformation. Hence, any force other than the shape restoring capillary force can easily deform the interface.

Vibration induced transition. Water channels with reduced volumes v corresponding to the upper limit of the bistability interval, with an error of 40 nL, (around point (ii) of Figure 1) are then prepared on the post. With the liquid in the homogeneous channel state, we turn on the vertical oscillations and record whether a transition to the bulge state is observed. The
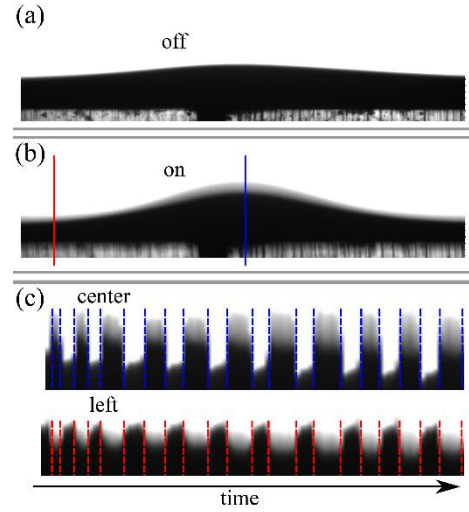

Figure 5 (a) Central part of a liquid drop on a short post with length-to-width ratio $\ell \simeq 15$ and a reduced liquid volume $v \approx 5.5$. (b) Liquid bulge for the same parameters as in (a) at a frequency $f = 500$ Hz and for an acceleration of $a = 255$ m/s^2. (c) Spatio-temporal diagrams of vertical cuts of the profile in the center and left side of the post, as indicated by solid lines in (b).

dynamical phase diagram of Figure 3 summarizes all the data taken. Each data point is the result of at least ten complete runs taken under the same nominal conditions. Full green circles (red squares) indicate that at that acceleration and frequency a transition is (is not) found. The dashed parabolic lines represent the sweeps of the diagram taken at constant amplitude. To facilitate the reading of the diagram, the regions where the transition is admitted and prohibited are colored in green and red, respectively. The white region corresponds to oscillation amplitudes too small to be accurately measured ($A < 4$ μm). It is evident from the diagram of Figure 3 that between 460 Hz and 530 Hz, it is not possible to induce the transition to the bulge state up to the maximum acceleration achievable with our shaker. In this gap of frequencies and amplitudes, the interface of the liquid channel undergoes strong irregular fluctuations resembling an overlay of several standing waves.

The transition from the homogeneous channel to the bulge morphology in the remaining region is irreversible: once the liquid is in the bulge state, it cannot be driven back to the homogeneous channel state by changing the amplitude or frequency, or even by turning off the shaker. In agreement with experimental and theoretical results, the bistability between the homogeneous and the bulged channel is not observed on relatively short posts.[14]

To illustrate this dynamical response of water interface, the diagram shown in Figure 3 is complemented with simultaneous lateral and frontal images of the channel taken at selected points of the phase diagram labeled by letters. Due to the finite exposure time, it is evident the complex evolution of the water profile and the excitation of oscillation modes, particularly for (a) and (c). In both cases, the vibrations induce a transition to the bulge state, while in (b) the liquid remains in the homogeneous channel state. These images and the movies loaded as Supplemental Material suggest that the transition is hindered by the excitation of standing capillary waves on the channel.

4

Inspection of the irregularly oscillating channels in the frequency gap of the dynamical phase diagram of Figure 3 shows that the local oscillation frequency of the waves fluctuates around the excitation frequency (see top snapshot of Figure 4).
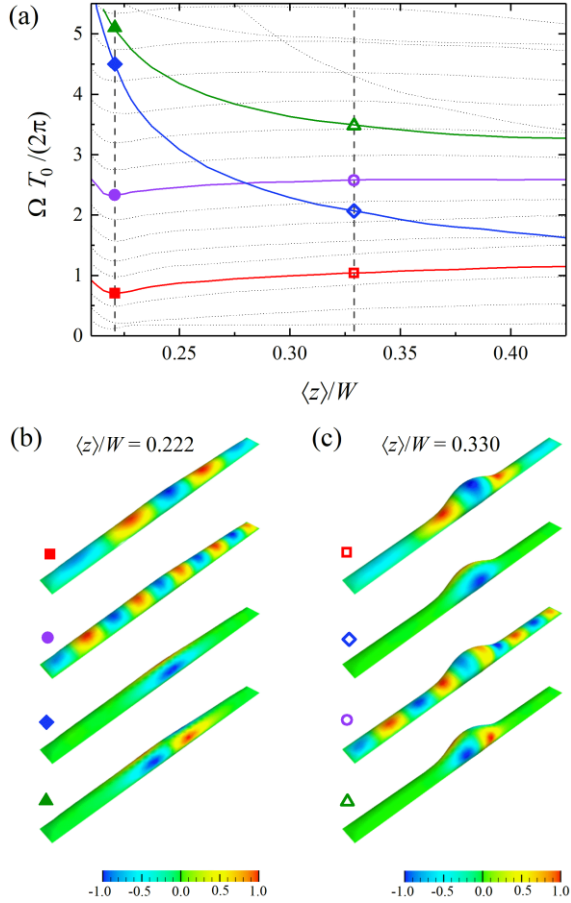
Figure 6 (a) Spectrum of numerically computed natural oscillation frequencies Ω of a liquid drop on a short post with $\ell =15$ and reduced volume of $v = 5.7$ as a function of the vertical center of mass position $\langle z\rangle/W$ in units of the capillary inertial time scale. Filled and open symbols are the natural oscillations modes of the liquid interface for $\langle z\rangle/W = 0.222$ (b) and $\langle z\rangle/W = 0.330$ (c), respectively. The local oscillation amplitude shown in the snapshots (b) and (c) is displayed by the corresponding color maps, which are constructed in terms of the maximum amplitude as described in Figure 3.

Hence, the observed standing capillary waves cannot be Faraday waves as they would oscillate at a frequency that is exactly half of the excitation frequency.[26] A closer look at the time slices of Figure referring to a vertical cut of the channel reveals that the oscillations are a superposition of a slow and a fast component. The frequency of the fast component correlates to the amplitude of the slow "sloshing" component. Generally, we find that the local frequency of the fast component is the higher, the lower the amplitude of the slow, irregularly fluctuating component.

Another example of a coupling of fast and slow degrees of freedom was observed on short posts with a length-to-width ratio $\ell \simeq 15 < \ell^*$. As explained above, the flat channel state

transforms continuously into a bulge state on short posts during volume growth and, consequently, a bistability between a bulge and channel state is not possible. In spite of the missing bistability, we still encounter a transformation of a flat channel into a bulge in response to vertical vibrations. At variance with experiments on long posts with liquid drops in the bi-stable region, the liquid on the short post is collected into the central region only if the vibration are switched on, c.f. the time slices shown in Figure 5. In contrast to long posts, this dynamically sustained liquid bulge decays quickly and returns to the flat, spread-out channel morphology after the vertical vibrations are stopped.

Dynamic lifting force. The transition of the vertically vibrated liquid channel into a permanent bulge on long posts, and the formation of a transient bulge on short posts can be captured in a simple model. In the present approach, we consider the coupling of the slow degree of freedom describing the transition between a channel and a bulge to fast interfacial oscillations in response to the vertical vibrations. Suitable coordinates to parameterize the slow degree of freedom is the vertical position of the center of mass $\langle z\rangle$. The natural frequencies of the oscillation modes Ω_i of the liquid interface, as well as the corresponding effective masses μ_i and spring constants k_i, are numerically computed from triangulated models of the free liquid interface obtained by energy minimizations are described in Supplemental Material.

For simplicity, we consider the limiting case of an inviscid incompressible fluid surrounded by vacuum, which allows us to assume potential flows in the bulk of the liquid and a full-slip boundary condition on the solid substrate. The decay length of the viscous boundary layer on the substrate $\delta = \sqrt{2\eta/(\rho f)}$ is computed to be $\delta \approx 0.08$ mm for the lowest frequency of 300 Hz, being small compared to the typical vertical extensions of the liquid bulges $H \lesssim 1$mm. This estimate is in accord with the observation of small damping in our experiments. Hence, it is useful to employ the capillary-inertial time scale $T_0 = \sqrt{\gamma/(\rho W^3)}$ to normalize all physical quantities together with the mass unit $M_0 = \rho W^3$, and length unit $L_0 = W$.

According to our experimental observations, only a few localized modes of the interface are excited on the bulge or within its direct vicinity. The majority of natural oscillation modes found in our numerical computations extend over the entire channel including also the flat regions of the liquid on the extremities of the bulge. Apart from the particular case of a driving frequency within the gap, oscillation modes that extend over the entire channel are not observed in experiments. Comparisons of the spectra for different length to width ratio of the post reveal that the oscillations frequencies of the localized modes, Ω_i, as well as the effective mass and springs constants of the oscillators, μ_i and k_i, are mainly governed by the size and extension of the bulge. Our minimal model of the oscillating bulges thus includes only the set of localized modes and their coupling to the slow degree of freedom described by the vertical center of mass position $\langle z\rangle$.
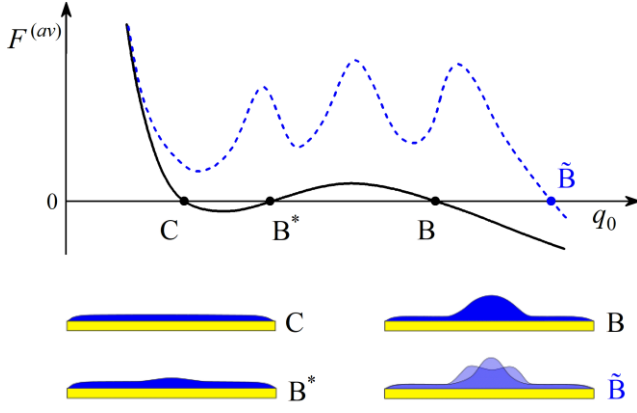
Figure 7 (Top) Schematic of the force landscape the homogeneous channel and bulge morphology experience in terms of the slow degree of freedom without oscillations (black solid line) and with driving by vertical vibrations (blue dashed line). (Bottom) stationary liquid morphologies on the post. Stable liquid channel (C), unstable saddle point (B*), stable bulge (B), and a dynamically stabilized bulge morphology ($\tilde{B}$).

Besides the external forcing and the conservative force $-\frac{\partial V_0}{\partial q_0}$ related the energy landscape discussed above, we encounter an effective force that couples to the amplitude of the standing capillary waves and to the derivatives of their respective spring constant and effective mass. If we assume that the oscillations of the modes are fast compared to the motion of the bulge, and display the same harmonic time dependence as the external forcing, the effective, time averaged force that acts on the bulge can be written in the form:

$$F^{(av)} = F_0 - \frac{1}{2}\sum_{i=1}^{N}\left(\frac{\partial k_i}{\partial q_0} - \omega^2 \frac{\partial \mu_i}{\partial q_0}\right)\overline{q_i^2} \tag{1}$$

where the over bar denotes the time average. A derivation of the time averaged force Eq. (1) is given in the supporting material.

A lifting force acting on sessile drops in the presence of vertical vibrations is described in Ref.[27] for a viscoelastic fluid. As shown in this work, the phenomenon can be qualitatively captured by a simple model that is in full analogy to Kapitza's pendulum[28]. At variance with Kapitza's model, we find that the dynamic force is proportional to the square of the amplitude of a resonant oscillation mode and not to the amplitude of the excitation itself. Unlike the model for the inverted pendulum, we consider a slow degree of freedom that couples to a number of fast degrees of freedom through a de-tuning of the resonances. To determine the sign of the dynamic force contribution to the effective force $F^{(av)}$, as described by the second term in Eq. (1) we consider the derivative of the square of the natural oscillations frequencies:

$$\frac{\partial \Omega_i^2}{\partial q_0} = \frac{1}{\mu_i}\left(\frac{\partial k_i}{\partial q_0} - \Omega_i^2 \frac{\partial \mu_i}{\partial q_0}\right) \tag{2}$$

and notice that we expect to find high amplitudes $\overline{q_i^2}$ for weakly damped oscillators around resonance $\omega \approx \Omega_i$ and, thus, a strong dynamic force. Inspection of Eq. (1) reveals that the dynamic force is positive, i.e. promoting the formation of a central bulge whenever the inequality $\frac{\partial \Omega_i^2}{\partial q_0} < 0$ holds.

Numerically computed natural frequencies of a drop on a short post as a function of the center of mass $\langle z \rangle$ shown in Figure 6 demonstrate that the frequencies of some modes indeed decrease strongly as the height $\langle z \rangle$ of the center of mass grows. Inspection of the examples shown in Figure 6(a) and (b) reveals that modes showing only a weak dependence on $\langle z \rangle$ extend over the entire post, while modes whose natural frequencies decay strongly with $\langle z \rangle$ display localized oscillation amplitudes in the center of the post.

The localized modes, if excited, contribute to a dynamic lifting force that pulls the liquid of the initially channel-like drop up in the center of the post. Such a dynamically sustained bulge forms only as long as the vibrations are switched on. Modes that extend over the entire length of the drop interface do not contribute to the dynamic lift force. Except for vibrations frequencies in the gap, the excitation of delocalized modes is not observed in our experiments, presumably due to significant viscous damping in the flat channels extending to either side of the central bulge.

The additional dynamic lifting force on the liquid created by the fast shape oscillations can trigger a global transition from a channel to a bulge morphology. When approaching the largest volume of a stable liquid channel on a long post with $\ell > \ell^* \approx 16$, the magnitude of the external force required to overcome the barrier between channel and bulge state becomes arbitrarily small,[14] as sketched in the force landscape in Figure 7. The evolution of the dynamic lifting force during volume growth is determined by the sequence of resonances of localized oscillation modes that appear on the bulge at a given excitation frequency of the vertical vibrations.

SUMMARY AND CONCLUSIONS

Experiments with drops wetting vertically vibrated long posts with $\ell = 36$ demonstrate that the channel-to-bulge transition can be triggered by vertical vibrations of the support if the liquid volume is close to the maximum volume of a mechanically stable channel. For this volume, the reverse transition from a bulge to a channel is never observed. This finding is supported by numerically computed energy landscapes of a drop on a post in terms of the vertical position $\langle z \rangle$ of the center of mass. In accordance with previous work,[14] we find that the energy landscape evolves from a single-well potential for short post $\ell < \ell^* = 16$ into a double-well potential for drops on long posts $\ell > \ell^* = 16$ and with volume v in the bi-stable range.

Our experiments also show that on a short post with $\ell = 15 < \ell^*$, the liquid may be collected into a central bulge during vibrations even though the length-to-width ratio ℓ and reduced volume v lies outside the range of mechanically bi-stable static shapes. In the latter case, the bulge exists only as long as the vertical vibrations of the post are switched on. To explain the

existence of dynamically sustained bulges, we propose a dynamic lifting force acting on the vertical coordinate $\langle z \rangle$ of the center of mass. A dynamic force arises in the presence of an ensemble of linear oscillators, here the standing capillary waves that are excited on the interface of the drop, that are detuned by the slow degree of freedom $\langle z \rangle$. A fast oscillation mode contributes to a positive force acting on the slow degree of freedom q_0 if the corresponding natural oscillation frequency Ω decreases with an increasing value of the coordinate q_0, here the height $\langle z \rangle$ of the center of mass above the post.

Numerical computations of the spectrum of natural oscillation modes and frequencies do not explain the existence of band of frequencies on long posts with $\ell = 36$ where the transition into a final bulge is not observed. However, in this range of excitation frequencies, our numerical computations are able to correctly capture the two oscillation modes on the final bulges at vibration frequencies above and below the band. These two modes display the same discrete symmetry and a superposition of them could lead to a scattering of the injected energy into various delocalized oscillation modes of the same discrete symmetry during the onset of the bulge formation.

ASSOCIATED CONTENS

Supporting information
Movie S1: Slow motion side view of channel-to-bulge transition occurring at $f = 640$ Hz and $a = 160$ m/s². Different oscillations modes can be observed as the liquid interface changes morphology. Once the forcing oscillations are turned off, the system remains in the bulge state.
Movie S2: Real time front view of channel-to bulge transition occurring at $f = 640$ Hz and $a = 160$ m/s². A normal oscillation mode of the final bulge state can be observed. Once the forcing oscillations are turned off, the system remains in the bulge state
Movie S3: At $f = 500$ Hz the channel-to-bulge transition does not occur and the system remains in the channel morphology.

AUTHOR INFORMATION

Corresponding authors
*E-mail: giampaolo.mistura@unipd.it
†E-mail: martin.brinkmann@physik.uni-saarland.de

Notes
The authors declare no conflict of interest.

ACKNOWLEDGEMENT

REFERENCES

(1)   Mugele, F.; Baret, J. C. Electrowetting: From Basics to Applications. *J. Physics-Condensed Matter* **2005**, *17* (28), R705–R774.

(2)   Latikka, M.; Backholm, M.; Timonen, J. V. I.; Ras, R. H. A. Wetting of Ferrofluids: Phenomena and Control. *Current Opinion in Colloid and Interface Science*. 2018, pp 118–129.

(3)   Daniel, S.; Chaudhury, M. K. Rectified Motion of Liquid Drops on Gradient Surfaces Induced by Vibration. *Langmuir* **2002**, *18* (9), 3404–3407.

(4)   Wixforth, A.; Strobl, C.; Gauer, C.; Toegl, A.; Scriba, J.; v. Guttenberg, Z. Acoustic Manipulation of Small Droplets. *Anal. Bioanal. Chem.* **2004**, *379* (7–8), 982–991.

(5)   Dong, L.; Chaudhury, A.; Chaudhury, M. K. Lateral Vibration of a Water Drop and Its Motion on a Vibrating Surface. *Eur. Phys. J. E* **2006**, *21* (3), 231–242.

(6)   Brunet, P.; Eggers, J.; Deegan, R. D. Vibration-Induced Climbing of Drops. *Phys. Rev. Lett.* **2007**, *99* (14), 144501.

(7)   Brunet, P.; Eggers, J.; Deegan, R. D. Motion of a Drop Driven by Substrate Vibrations. *Eur. Phys. Journal-Special Top.* **2009**, *166*, 11–14.

(8)   Noblin, X.; Kofman, R.; Celestini, F. Ratchetlike Motion of a Shaken Drop. *Phys. Rev. Lett.* **2009**, *102* (19), 194504.

(9)   Yeo, L. Y.; Friend, J. R. Surface Acoustic Wave Microfluidics. *Annu. Rev. Fluid Mech. Vol 46 2014*, *46*, 379–406.

(10)   Sartori, P.; Quagliati, D.; Varagnolo, S.; Pierno, M.; Mistura, G.; Magaletti, F.; Casciola, C. M. Drop Motion Induced by Vertical Vibrations. *New J. Phys.* **2015**, *17*, 113017.

(11)   Foresti, D.; Nabavi, M.; Klingauf, M.; Ferrari, A.; Poulikakos, D. Acoustophoretic Contactless Transport and Handling of Matter in Air. *Proc. Natl. Acad. Sci.* **2013**, *110* (31), 12549–12554.

(12)   Azad, M. A. K.; Ellerbrok, D.; Barthlott, W.; Koch, K. Fog Collecting Biomimetic Surfaces: Influence of Microstructure and Wettability. *Bioinspir. Biomim.* **2015**, *10* (1), 016004.

(13)   Brinkmann, M.; Lipowsky, R. Wetting Morphologies on Substrates with Striped Surface Domains. *J. Appl. Phys.* **2002**, *92* (8), 4296–4306.

(14)   Ferraro, D.; Semprebon, C.; Tóth, T.; Locatelli, E.; Pierno, M.; Mistura, G.; Brinkmann, M. Morphological Transitions of Droplets Wetting Rectangular Domains. *Langmuir* **2012**, *28* (39), 13919–13923.

(15)   Ledesma-Aguilar, R.; Nistal, R.; Hernández-Machado, A.; Pagonabarraga, I. Controlled Drop Emission by Wetting Properties in Driven Liquid Filaments. *Nat. Mater.* **2011**, *10* (5), 367.

(16)   Ghosh, A.; Ganguly, R.; Schutzius, T. M.; Megaridis, C. M. Wettability Patterning for High-Rate, Pumpless Fluid Transport on Open, Non-Planar Microfluidic Platforms. *Lab Chip* **2014**, *14* (9), 1538–1550.

(17)   Kligner, A.; Mugele, F. Electrowetting-Induced Morphological Transitions of Fluid Microstructures. *J. Appl. Phys.* **2004**, *95* (5), 2020–2918.

(18)   Eral, H. B.; de Ruiter, J.; de Ruiter, R.; Oh, J. M.; Semprebon, C.; Brinkmann, M.; Mugele, F. Drops on Functional Fibers: From Barrels to Clamshells and Back. *Soft Matter* **2011**, *7* (11), 5138–5143.

(19)   Sauret, A.; Bick, A. D.; Duprat, C.; Stone, H. A. Wetting of Crossed Fibers: Multiple Steady States and Symmetry Breaking. *EPL (Europhysics Lett.* **2014**, *105* (5), 56006.

(20)   Broesch, D. J.; Frechette, J. Fabrication and Visualization of Capillary Bridges in Slit Pore Geometry. *J. Vis. Exp.* **2014**, *83*, e51143–e51143.

(21)   Dokowicz, M.; Nowicki, W. Morphological Transitions of Droplets Wetting a Series of Triangular Grooves. *Langmuir* **2016**, *32* (28), 7259–7264.

(22)   Patrick Jansen, H.; Sotthewes, K.; Zandvliet, H. J. W.; Kooij, E. S. Potential of Lattice Boltzmann to Model Droplets on Chemically Stripe-Patterned Substrates. *Appl. Surf. Sci.* **2016**, *361*, 122–132.

(23)   Gau, H.; Herminghaus, S.; Lenz, P.; Lipowsky, R. Liquid Morphologies on Structured Surfaces: From Microchannels to Microchips. *Science (80-.).* **1999**, *283* (5398), 46–49.

(24)   Schäfle, C.; Brinkmann, M.; Bechinger, C.; Leiderer, P.; Lipowsky, R. Morphological Wetting Transitions at Ring-Shaped Surface Domains. *Langmuir* **2010**, *26* (14), 11878–11885.

(25)   Brigo, L.; Carofiglio, T.; Fregonese, C.; Meneguzzi, F.; Mistura, G.; Natali, M.; Tonellato, U. An Optical Sensor for PH Supported onto Tentagel Resin Beads. *Sensors Actuators B Chem.* **2008**, *130* (1), 477–482.

(26)   Douady, S. Experimental Study of the Faraday Instability. *J. Fluid Mech.* **1990**, *221*, 383–409.

(27)   Ramachandran, R.; Nosonovsky, M. Vibro-Levitation and Inverted Pendulum: Parametric Resonance in Vibrating Droplets and Soft Materials. *Soft Matter* **2014**, *10* (26), 4633–4639.

(28)   Kapitza, P. L. Dynamic Stability of the Pendulum with Vibrating Suspension Point. *Sov. Phys. JETP* **1951**, *21*, 588–597.

TABLE OF CONTENTS